

# The Evolution of Morphology and Properties of Films Obtained by Anodizing Zirconium

DANIELA IONITA, ADRIAN NICOARA, ANDREI BOGDAN STOIAN\*

University Politehnica of Bucharest, Faculty of Applied Chemistry and Materials Science, 1-7 Gheorghe Polizu Str., 011061, Bucharest, Romania.

*By anodizing zirconium in phosphoric acid at various potentials, different structures were obtained on the surfaces of the samples. The morphologies and compositions of the obtained coatings were investigated using scanning electronic microscopy (SEM), X-rays analysis (XRD) and Raman spectroscopy and were found to be dependent on anodizing potential. Electrochemical tests were performed in order to establish the stability of the samples. The film delamination forces increased with the anodizing potential, confirming that the zirconium dioxide film formed during anodizing becomes more resistant at higher potentials.*

*Keywords: anodizing; zirconium phosphate; SEM; adhesion*

Due to low cross section for neutron absorption, remarkable resistance to corrosion in numerous aggressive media simultaneously with mechanical properties at elevated temperatures and high dielectric constant, Zirconium (Zr) has been extensively used in nuclear industry, microelectronic applications and catalysis [1-3]. Responsible for such properties is the natural passive oxide named *zirconia* which makes a protective stratum barrier [4], and can be tailored by the anodizing conditions, using the same mechanism as for titanium [5]. In the last years, microstructural characterization of Zr alloys with titanium and other valve metals has been deeply investigated for their potential mechanical and biomedical applications [6, 7]. Previous studies [8] have shown that anodizing Zr in  $H_3PO_4$  produces apart from  $ZrO_2$ , a superficial stratum rich in phosphates and other studies revealed [9] that the phosphates are usually formed as zirconium hydrogen phosphate ( $Zr(HPO_4)_2 \cdot H_2O$ ), alpha phase ( $\alpha$ -ZP) being the more common.

The aim and novelty of the present manuscript was the fabrication of micro architectures on Zr via anodizing in phosphoric acid ( $H_3PO_4$ ) and the methodical investigation of the surface properties at various potential using a variety of methods and physical concepts. The surface analysis and compositions of films were correlated with the macrostructure properties able to induce their use in applications such as: drug delivery [10, 11] catalysis [12] or nuclear waste management [13].

## Experimental part

Zr samples were cut to size ( $5 \times 1$  cm, thickness 0.1mm) and then were cleaned in distilled water and ethanol for 10 min each by ultrasonication. The samples were then anodized at 5 V, 15 V, 45 V and 75 V using a Matrix MPS-7163 DC power supply in an aqueous electrolyte containing 2 M  $H_3PO_4$  (85 wt.%) and 30 mM NaF for 60 min each.

The surface morphology was investigated with a Quanta 650 scanning electron microscope (SEM) from FEI in high vacuum at 10kV.

Identification of phases by XRD analysis was performed with a Shimadzu XRD 6000 equipment with Cu K radiation ( $\lambda = 1.5406 \text{ \AA}$ ). These patterns were scanned in steps of  $0.02^\circ$  ( $2\theta$ ) from 5 to 70 degrees.

Crystalline domains presence in the anodic oxides as determined by Raman spectroscopy using a Horiba Lab

Raman Evolution instrument. The acquisition was performed using a 514 nm argon laser with a  $50\times$  objective lens and measured power  $68.7 \mu W$ . Acquisition time was 3 s with 20 superpositions. The incorporation of species with P and O from the anodizing electrolyte was put in evidence [14].

The electrochemical tests were performed using an Autolab PGSTAT 302N in a conventional three electrode system with Zr samples as working electrodes, Pt foil as counter electrode and Ag/AgCl reference electrode, using as electrolyte Afnor artificial saliva with the composition (g/L): NaCl 0.7; KCl 1.2;  $Na_2HPO_4$  0.26;  $NaHCO_3$  1.5; KSCN 0.33;  $CO(NH_2)_2$  1.35 [15]. Before each measurement, the potential was left to stabilize for 10 min at open circuit. Polarization data were registered between  $\pm 200$  mV and OCP using a scan rate of 0.2 mV/s. Electrochemical data were evaluated and fitted using Nova 1.10 software.

The film-substrate bond strength was evaluated form film detachment experiments carried out with PosiTest AT-M adhesion tester form DeFelsko using 10 mm diameter aluminum dollies.

## Results and discussions

### Surface characterization

The evolution of the morphology of the anodized Zr samples is presented in figure 1. At 5 V, semispheres with diameters of around 250-300 nm were formed in clusters. We think that these formations are composed of  $ZrO_2$  produced during anodizing. Small ridged structures of  $\alpha$ -ZP were found scattered on the surface. At 15 V the diameter of the  $ZrO_2$  semispheres decreases to around 240 nm. These formations are more tightly packed than at 5 V, hinting to the formation of a more compact oxide layer. More  $\alpha$ -ZP structures were formed at this voltage, but they are less defined and start to self organize to take their classical flaked, laminar and aggregated shapes. Anodizing at 45 V led to the total coverage of the sample surface with  $\alpha$ -ZP structures. The aggregated quasi-hexagonal pellet structures had lengths of around 600 nm and thicknesses of around 80 nm were not ordered in any particular direction. Both  $\alpha$ -ZP structures and porous  $ZrO_2$  were visible on the surface of the sample when increasing the potential at 75 V.  $\alpha$ -ZP structures were found as laminated aggregates with lengths ranging between 0.17-1 $\mu m$  and thicknesses

\* email: andreibstoian@yahoo.com, Phone: +40 21 402 3930

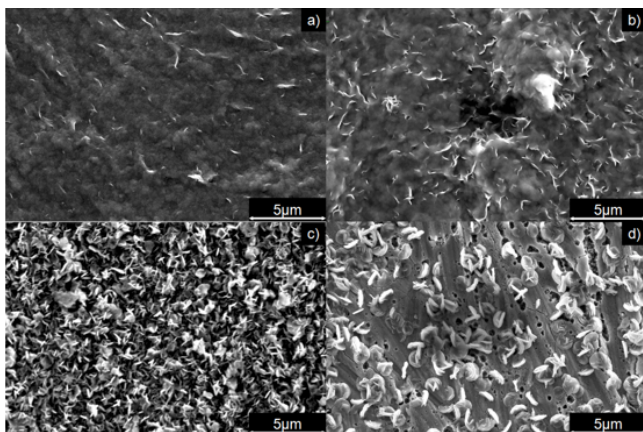


Fig. 1. SEM microscopy images for anodized Zr at 5 V a); 15 V b); 45 V c); 75 V d)

between 20-150 nm. The  $ZrO_2$  pores present on the surface had diameters of 100-400 nm.

The patterns obtained by XRD (fig. 2) were matched with relevant ASTM Cards for identification. Compounds with P and O such as  $Zr_3(PO_4)_4$ ,  $(Zr(HPO_4)_2 \cdot H_2O)$ , and  $ZrP_2O_7$  are present with different intensity peaks together with Zr and  $ZrO_2$ . The introduction of phosphorus compounds onto the oxide markedly enhances the acidic properties, regardless of the type of phosphate compounds XRD clearly showed some peaks, which correspond to crystallized  $ZrO_2$  structures, such as monoclinic phase  $ZrO_2$  (m- $ZrO_2$ ) and traces of tetragonal phase  $ZrO_2$  (t- $ZrO_2$ ) [16]. At lower potentials  $ZrO_2$  peaks are more clearly defined, but at higher potentials the peaks are smaller and the phosphate compounds peaks are more evident [17]. Peaks at  $34.76^\circ$ ;  $36.46^\circ$ ;  $63.49^\circ$ ;  $68.46^\circ$  and  $69.50^\circ$  corresponding to Zr appear in all samples together with  $30.31^\circ$ ;  $35.05^\circ$ ;  $50.52^\circ$  and  $60.11^\circ$  attributed to  $ZrO_2$  [18], but for each potential their intensities are different and, in some cases, they appear in the same regions with peaks for phosphate compounds. At 5V the predominant phosphate compounds are  $Zr_3(PO_4)_4$  and  $ZrP_2O_7$ . Peaks corresponding for more acidic components as  $(Zr(HPO_4)_2 \cdot H_2O)$ , are predominant at samples elaborated at 75V.

The peaks at  $34.91$  and  $36.55^\circ$ , more evident at 45 V elaboration voltage, could be attributed to orthorhombic  $ZrO_2$ . Some reports state that a mixture of crystallized tetragonal phase (t- $ZrO_2$ ) and a monoclinic phase  $ZrO_2$  (m- $ZrO_2$ ) could be detected [16, 17] and such results are consistent with our data from Raman spectra.

The Raman results are presented in table 1 which is a summary of Raman shifts for studied samples.

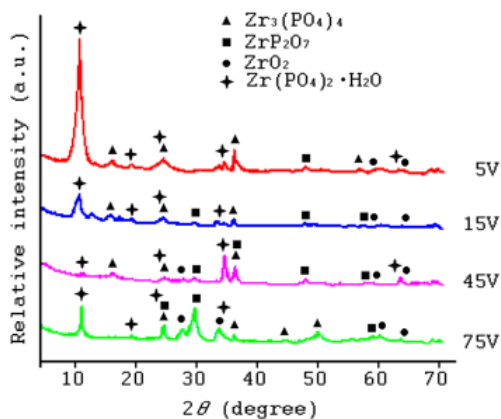


Fig. 2. XRD spectra for the anodized Zr obtained at different potentials

Table 1

RAMAN BANDS OF ANODIZING SAMPLES AT VARIOUS POTENTIALS

Potential \ Band	5V	15V	45V	75V
m $ZrO_2$	103	103	103	103
m $ZrO_2$	-	177	177	178
t $ZrO_2$	145	-	-	-
m $ZrO_2$	205	-	-	-
vas(P-O-P)	282	282	284	286
m $ZrO_2$	-	329	332	330
m $ZrO_2$	-	375	378	375
$\delta_s(PO_3)$	412	410	-	-
m $ZrO_2$	-	472	476	472
P-O-P	514	509	514	514
$\delta AS(PO_3)$	545	546	545	550
$\delta AS(PO_3)$	578	572	571	569
t $ZrO_2$	659	617	619	617
m $ZrO_2$	-	691	679	697
vs (P-O-P)	760	-	-	-

The anodic film at all studied potentials present common peaks at 103, 177, 329, 378, 476, 569  $cm^{-1}$ . Although the bands are relatively broad and have a shift of around 2.3  $cm^{-1}$  with respect to the spectrum of native oxide, most of them can be assigned to predominant monoclinic  $ZrO_2$  [19] and tetragonal traces. For samples elaborated at 5 V the important characteristic monoclinic band at 177  $cm^{-1}$  is missing, but the bands at 617 and 659  $cm^{-1}$  are evident for monoclinic and tetragonal  $ZrO_2$ . More bands characteristic for phosphoric compounds are present at 412  $cm^{-1}$ . The incorporation of species with P and O from the anodizing electrolyte may be one reason for the broad peaks of the Raman spectra in some regions, as was discussed in literature [14].

#### Polarization tests

The polarization data recorded for the anodized samples are represented as Tafel plots (fig. 3) and the corrosion parameters obtained after fitting are listed in table 2. The anodized samples were compared to polished Zr.

The corrosion potential of the anodized samples is more positive than that recorded for polished Zr, and is shifted to more electropositive values with the increase of the anodizing potential to a stable value. The corrosion resistance improves slightly at lower potentials and experiences a drastic improvement when the anodizing potential reaches 75 V.

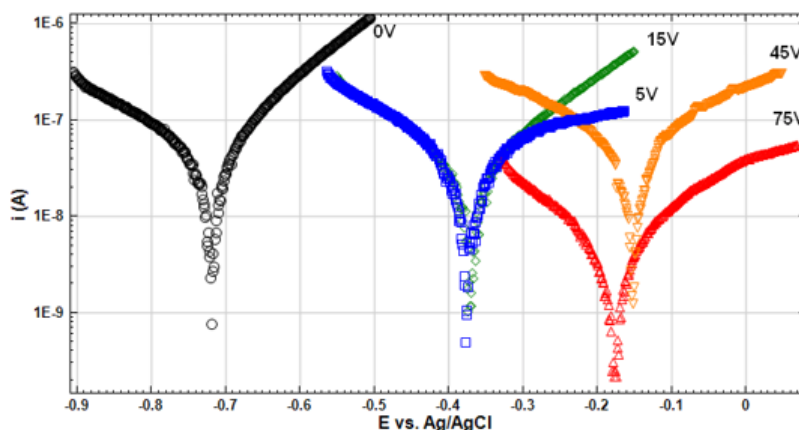


Fig. 3. Tafel plots for polished (0 V) and anodized Zr at different potentials (5 V, 15 V, 45 V, 75 V)

Sample	0 V	5 V	15 V	45 V	75 V
E <sub>cor</sub> (mV)	-719	-377	-364	-147	-173
j <sub>cor</sub> (nA/cm <sup>2</sup> )	35.2	38.2	22.4	17.6	3.58
Corrosion rate (μm/year)	0.97	0.86	0.5	0.39	0.08
Polarization resistance (MΩ)	0.73	1.07	1.1	1.79	6.93

**Table 2**  
ELECTROCHEMICAL PARAMETERS FOR POLISHED AND ANODIZED Zr

### Film detachment forces

The film detachment forces were measured when the obtained film was removed from the Zr foil surface. The film detachment force increases with the increase of the potential (fig. 4).

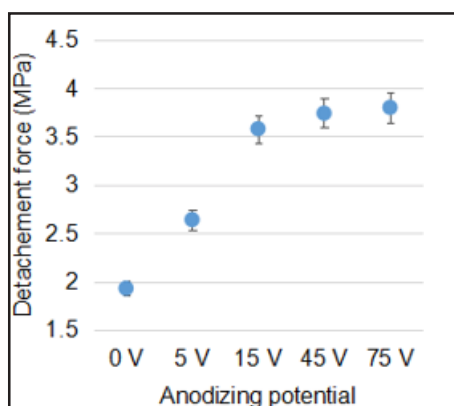


Fig. 4. Detachment forces for Zr samples obtained at various potentials

It follows that ZrO<sub>2</sub> deep film formed during anodizing becomes more resistant at higher potentials. This difference in strength indicates that for films obtained at higher potentials, ZrO<sub>2</sub> acts as a binding layer between the metallic substrate and α-ZP structures, thereby conferring improved interfacial mechanical strength.

### Conclusions

Using SEM, the microstructures of ZrO<sub>2</sub> and α-ZP coatings obtained after Zr anodizing in H<sub>3</sub>PO<sub>4</sub> at 5 V, 15 V, 45 V and 75 V were determined to be directly influenced by the applied potential. When a higher anodizing potential was used, more well organized and complex structures were formed on the surface. Raman, and XRD investigations showed that the films were formed from different zirconium oxides and phosphates. The films are formed mainly from monoclinic phases with traces of tetragonal phases. The electrochemical tests revealed that using higher anodizing potentials leads to highly stable surfaces. The evaluation of the delamination forces revealed that the ZrO<sub>2</sub> deep film formed during the anodizing becomes more resistant at higher potentials. These experiments enabled the understanding the optimal parameters needed for the development of damage-tolerant thin films leading to practical applications.

*Acknowledgments:* This work was supported by CNCISIS-UEFISCSU, project number PN-III-P4-ID PCE 2016-0316.

### References

- DEACONU, M., CIUCA, I., MELEG, T., MIHALACHE, M., DINU, A., Rev. Chim. (Bucharest), **67**, no. 7, 2016, p. 1161.
- GOMEZ SANCHEZ, A., KATUNAR, M., SCHREINER, W., DUFFO, G., CERE, S., SCHIFFRIN, D., Acta. Chim. Slov., **61**, No.2, 2014, p. 316.
- SPIELBAUER, D., MEKHEMER, G., RIEMER, T., ZAKI, M., KNÖZINGER, H. J. Phys. Chem. B, **101**, No. 23, 1997, p. 4681.
- HANAWA, T., TSUTSUMI, Y. Bioceram. Dev. Appl., **1**, 2010, article ID D110119.
- DUMTRIU, C., POPESCU, M., VOICU, G., DEMETRESCU, I. Rev. Chim. (Bucharest), **64**, no. 6, 2013, p. 599.
- BOLAT, G., IZQUIERDO, J., SANTANA, J., MARECI, D., SOUTO, M.R. Electrochim. Acta, **88**, No. 29, 2013, p. 447.
- STOIAN, A.B., VARDAKI, M., IONITA, D., ENACHESCU, M., PRODANA, M., BRANCOVEANU, O., DEMETRESCU, I. Ceram. Internat. **44**, No. 6, 2018, p. 7026.
- ROMONTI, D.E., GOMEZ SANCHEZ, A., MILOSEV, I., DEMETRESCU, I., CERE, S. Mater. Sci. Eng. C, **62**, 2016, p. 458.
- GENOVEVA, G., ENRIQUE, O., TERESITA, R., EDUARDO, O., JMMCE, **6**, No. 1, 2007, p. 39
- DIAZ, A., DAVID, A., PEREZ, R., GONZALEZ, M.L., BAEZ, A., WARK, S.E., ZHANG, P., CLEARFIELD, A., COLON, J.L., Biomacromolecules, **11**, No. 9, 2010, p. 2465.
- TANG, S., HUANG, X., CHEN, X., ZHENG, N., Adv. Func. Mater. **20**, No. 15, 2010, p. 2371.
- COSTANTINO, U., MARMOTTINI, F., CURINI, M., ROSATI, O. Catal. Lett., **22**, No. 4, 1993, p. 333.
- SCHEETZ, B.E., AGRAWAL, D.K., BREVAL, E., ROY, R., Waste Manag., **14**, No. 6, 1994, p. 489.
- DÍAZ, A., SAXENA, V., GONZALEZ, J., DAVID, A., CASANAS, B., CARPENTER, C., BATTEAS, J. D. COLÓN, J. L., CLEARFIELD, A., HUSSAIN, M. D. Chem. Commun., **48**, No. 12, 2012, p. 1754.
- DILEA, M., MAZARE, A., IONITA, D., DEMETRESCU, I. Mater. Corros., **64**, No. 6, 2013, p. 493.
- MEKHEMER, G. A. H., Colloid. Surface. A, **141**, No. 2, p. 227
- GUO, L., ZHAO, J., WANG, X., XU, R., LU, Z., LI, Y. Mater. Sci. Eng. C, **29**, No. 4, 2009, p. 1174.
- GOWRI, S., RAJIV GANDHI, R., SUNDRARAJAN, M., J. Mater. Sci. Technol., **30**, No. 8, 2014, p. 728.
- KUMARI, L., DU, G. H., LI, W. Z., VENNILA, R. S., SAXENA, S. K., WANG, D. Z. Ceram. Int. **35**, No. 9, 2009, p. 2401.

Manuscript received: 16.01.2019